Impacts of carrier capture and relaxation rates on the modulation response of injection-locked quantum dot lasers

Cheng Wang[a*], Frédéric Grillot[a,b] and Jacky Even[a]

[a]Université Européenne de Bretagne, INSA, CNRS FOTON, 20 avenue des buttes de Coesmes, 35708 Rennes Cedex 7, France
[b]Telecom Paristech, Ecole Nationale Supérieure des Télécommunications, CNRS LTCI, 46 rue Barrault, 75013 Paris, France

ABSTRACT

Taking into account the carrier dynamics in the wetting layer, excited state and the ground state, the intensity modulation properties of an injection-locked quantum dot laser are studied theoretically through a semi-analytical approach. It is demonstrated that both high carrier capture and relaxation rates enhance the modulation bandwidth as well as the resonance-peak amplitude. Moreover, the pre-resonance dip arising under positive detuning can be eliminated as well, which is beneficial for further bandwidth enhancement. It is also found that a large capture time reduces both the resonance frequency and the damping factor while both are increased by a large relaxation time.

Keywords: semiconductor laser, quantum dot, nonlinear dynamics, injection-locking

1. INTRODUCTION

Optical injection locking is an attractive technique for improving the performance of directly-modulated semiconductor laser, such as bandwidth enhancement [1], [2], reduction of relative intensity noise (RIN) and frequency chirp [3]-[6]. Although most relevant work has been conducted on quantum well (QW) lasers, the inclusion of quantum dots (QD) in the laser active media are more promising because of the 3-D confinement of carriers. The latter can substantially improve the laser properties so as to obtain a lower threshold current, a stronger temperature insensitivity and a reduced linewidth enhancement factor (LEF) [7]-[10]. In contrast to their QW counterparts, QD lasers have a more complex carrier dynamics due to the existence of wetting layer (WL) and excited states (ES). It is known that carrier lifetimes have significant influences on the dynamics of free-running QD lasers [11], [12]. In our previous work, it has been demonstrated that finite carrier capture time from the WL to the ES associated with the finite carrier relaxation time from the ES to the ground state (GS) as well as the Pauli blocking lead to the limitation of the modulation bandwidth [11]. Recently, Lingnau *et al* studied the impacts of the effective charge carrier scattering lifetimes on relaxation oscillation frequency and damping factor. Three dynamical regimes are identified, which are characterized by the level of synchronization between carrier dynamics in QDs and the WL [12]. Regarding optical injection-locked QD lasers, Naderi *et al* experimentally investigated the microwave properties based on a novel modulation transfer function incorporating the gain compression effect [1]. Theoretically, considering the carrier dynamics between the WL and the QDs, Pausch *et al* proposed an injection-locked QD laser model with which the bifurcation scenarios and the turn-on dynamics are studied numerically, and the influences of the nonlinear carrier lifetimes are analyzed [13]. Moreover, self-pulsation and excitability in optically injected QD lasers have been investigated accounting for excited states both theoretically and experimentally by Olejniczak *et al* [14]. In this paper, taking into account the carrier dynamics of WL, ES and GS [15]-[18], the impacts of carrier capture and relaxation rates on the intensity modulation (IM) properties of an injection-locked QD laser are studied theoretically through a semi-analytical approach. It is found that both large capture and relaxation rates enhance the 3-dB bandwidth. Moreover, the resonance peak amplitude is enlarged as well. Particularly, under positive detuning small capture and (or) relaxation times can eliminate the appearance of pre-resonance dip, which is the main source of limitations on the modulation bandwidth. It is also proved that large capture time reduces both the resonance frequency and the damping factor while those are increased by large relaxation time.

* cheng.wang@insa-rennes.fr; phone +33 223238464;

Physics and Simulation of Optoelectronic Devices XXI, edited by Bernd Witzigmann, Marek Osinski, Fritz Henneberger, Yasuhiko Arakawa, Proc. of SPIE Vol. 8619, 861908 · © 2013 SPIE
CCC code: 0277-786X/13/$18 · doi: 10.1117/12.2001929

2. RATE EQUATION MODEL DESCRIPTION

Figure 1 illustrates the typical scheme of an injection-locked QD laser. In the numerical model, the QD system is assumed to be in excitonic energy states, namely the electrons and holes are treated as electron-hole (e-h) pairs. The QD ensemble includes two energy levels: a two-fold degenerate GS and a four-fold degenerate ES. Figure 1 also shows the carrier dynamics in the QD laser. Carriers are supposed to be directly injected from contacts into the WL. Then they are captured into the ES within a capture time of τ_{ES}^{WL}, followed by the relaxation into the GS within a relaxation time of τ_{GS}^{ES}. On the other hand, carriers can also escape from the GS (τ_{ES}^{GS}) and ES (τ_{WL}^{ES}), which is governed by the Fermi distribution assumption as follows [19]:

$$\tau_{WL}^{ES} = 4\tau_{ES}^{WL}\frac{N_B / S_{QD}}{\rho_{WL}}\exp\left(\frac{E_{WL}-E_{ES}}{K_B T}\right) \tag{1}$$

$$\tau_{ES}^{GS} = \frac{1}{2}\tau_{GS}^{ES}\exp\left(\frac{E_{ES}-E_{GS}}{K_B T}\right) \tag{2}$$

where N_B is the QD number, S_{QD} is the total QD surface area. ρ_{WL} is the effective density of state in the WL. E_X is the energy with X denoting WL, ES and GS. Besides, some carriers recombine spontaneously with a spontaneous time of τ_X^{spon}. Stimulated emission occurs from the GS, and that from the ES is not taken into account in the model.

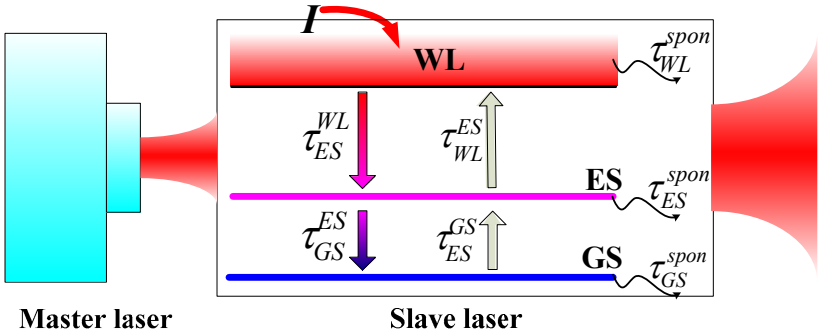

Figure 1. Schematic of injection-locked QD laser, and the carrier dynamics in the slave laser.

Following the sketch of figure 1, the rate equations for the injection-locked QD lasers can be written as:

$$\frac{dN_{WL}}{dt} = \frac{I}{q} + \frac{N_{ES}}{\tau_{WL}^{ES}} - \frac{N_{WL}}{\tau_{ES}^{WL}}f_{ES} - \frac{N_{WL}}{\tau_{WL}^{spon}} \tag{3}$$

$$\frac{dN_{ES}}{dt} = \frac{N_{WL}}{\tau_{ES}^{WL}}f_{ES} + \frac{N_{GS}}{\tau_{ES}^{GS}}f_{ES} - \frac{N_{ES}}{\tau_{WL}^{ES}} - \frac{N_{ES}}{\tau_{GS}^{ES}}f_{GS} - \frac{N_{ES}}{\tau_{ES}^{spon}} \tag{4}$$

$$\frac{dN_{GS}}{dt} = \frac{N_{ES}}{\tau_{GS}^{ES}}f_{GS} - \frac{N_{GS}}{\tau_{ES}^{GS}}f_{ES} - \frac{N_{GS}}{\tau_{GS}^{spon}} - \Gamma_p v_g g_{GS} S_{GS} \tag{5}$$

$$\frac{dS_{GS}}{dt} = (\Gamma_p v_g g_{GS} - \frac{1}{\tau_P})S_{GS} + \Gamma_p \beta_{SP}\frac{N_{GS}}{\tau_{GS}^{spon}} + 2k_c\sqrt{S_{inj}S_{GS}}\cos\phi \tag{6}$$

$$\frac{d\phi}{dt} = \frac{\alpha_H}{2}(\Gamma_p v_g g_{GS} - \frac{1}{\tau_p}) - \Delta\omega_{inj} - k_c\sqrt{\frac{S_{inj}}{S_{GS}}}\sin\phi \tag{7}$$

where N_X is carrier number, S_{GS} is photon number from the GS, and ϕ is the phase difference between the slave and master lasers defined as $\phi = \phi_{slave} - \phi_{master}$. The GS gain is given by

$$g = a_{GS}\left(N_{GS} - N_B\right)/V_{QD} \tag{8}$$

with a_{GS} the differential gain and V_{QD} the total volume of QDs. The Pauli blocking factors are given by

$$f_{GS} = 1 - \frac{N_{GS}}{2N_B};\ f_{ES} = 1 - \frac{N_{ES}}{4N_B} \tag{9}$$

Finally k_c denotes the coupling coefficient which is calculated by

$$k_c = \frac{v_g}{2L}\frac{1-R}{\sqrt{R}} \tag{10}$$

with v_g the group velocity, L the cavity length and R the facet reflectivity. The detuning frequency is defined by $\Delta\omega_{inj} = \omega_{master} - \omega_{slave}$. S_{inj} is the injected photon number and the injection ratio is R_{inj}=S_{inj}/S_{FE}, where S_{FE} is the photon number of the free-running laser . The LEF is denoted by α_H, τ_p is the photon lifetime, Γ_p is the optical confinement factor and β_{sp} is the spontaneous emission factor.

In order to obtain the laser's small-signal response to a sinusoidal current modulation $I_1 e^{j\omega t}$ around the bias current I_{bias}, let us assume solutions of the following form

$$\begin{aligned} dN_X &= N_{X1} e^{j\omega t} \\ dS_{GS} &= S_{GS1} e^{j\omega t} \\ d\phi &= \phi_1 e^{j\omega t} \end{aligned} \tag{11}$$

Following the standard approach of deriving the differential rate equations [20], the modulation transfer function can be extracted as follows:

$$H(\omega) = \frac{S_{GS1}(\omega)/I_1(\omega)}{S_{GS1}(0)/I_1(0)} = \frac{p_1 p_2 p_3 p_4 p_5}{z_1}\frac{(j\omega - z_1)}{\prod_{i=1}^{5}(j\omega - p_i)} \tag{12}$$

where z_1 is the unique zero, and the poles $p_1 \sim p_5$, which are also eigenvalues, are obtained from the determinant of the coefficient matrix in the differential rate equation. Let us note that these eigenvalues are important for the stability analysis of the bifurcation diagrams as well as for the extraction of the resonance frequency and the damping factor. As discussed in the following sections, the knowledge of the poles and zeros are also useful for analyzing the modulation response behaviours with respect to the Bode plot.

Table 1. Material and laser parameters (after [15]-[18], [21])

Symbols	Parameters	Values	Symbols	Parameters	Values
E_{WL}	WL energy	0.97 eV	n_r	Refractive index	3.27
E_{ES}	ES energy	0.87 eV	L	Active region length	0.05 cm
E_{GS}	GS energy	0.82 eV	W	Active region width	4×10^{-4} cm
τ_{ES}^{WL}	Capture time from WL to ES	12.6 ps	N	Number of QD layers	5
τ_{GS}^{ES}	Relaxation time from ES to GS	3.5 ps	N_D	QD density	1×10^{11} cm^{-2}
τ_{WL}^{spon}	Spontaneous time of WL	500 ps	Γ_p	Optical confinement factor	0.06
τ_{ES}^{spon}	Spontaneous time of ES	500 ps	β_{SP}	Spontaneous emission factor:	1×10^{-4}
τ_{GS}^{spon}	Spontaneous time of GS	1200 ps	α_i	Internal modal loss	6 cm^{-1}
a_{GS}	Differential gain of GS	5×10^{-15} cm^2	R_1=R_2	Mirror reflectivity	0.32
α_H	LEF	1.3			

3. RESULTS AND DESCUSSIONS

All the parameters used in the simulations are listed in table 1 unless stated otherwise. Firstly, we studied the steady-state properties of the QD laser as depicted in figure 2. The calculated current threshold for the free-running laser is I_{th}=54 mA. Above threshold simulations show that under optical injection operation with R_{inj}=0.5 at zero detuning condition, the

photon number is enhanced while carrier numbers in the GS and the ES are both reduced, nevertheless, the carrier number in the WL is little changed. In the following sections, the bias current of the slave laser and the injection level are set at I_{bias}=1.1 I_{th} and R_{inj}=0.5, respectively.

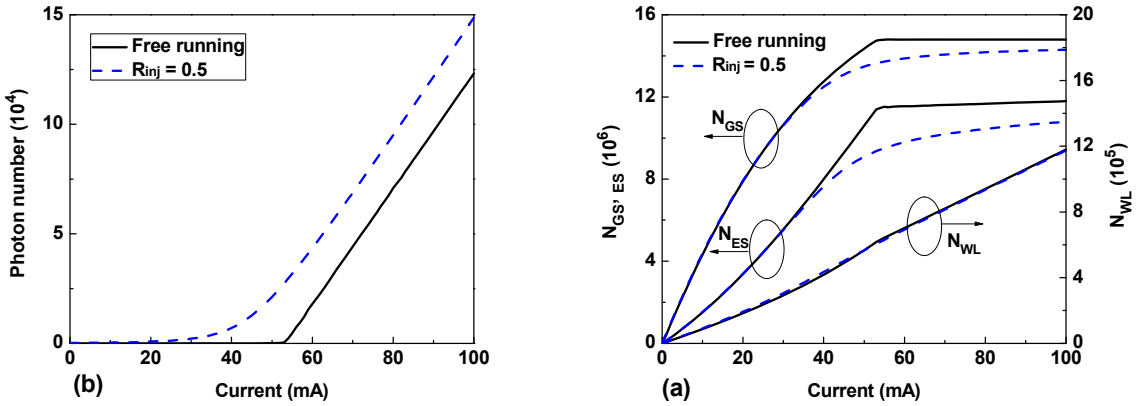

Figure 2. Steady state results versus pump current at zero detuning: (a) photon numbers of GS; (b) carrier numbers of GS, ES and WL under various injection ratios.

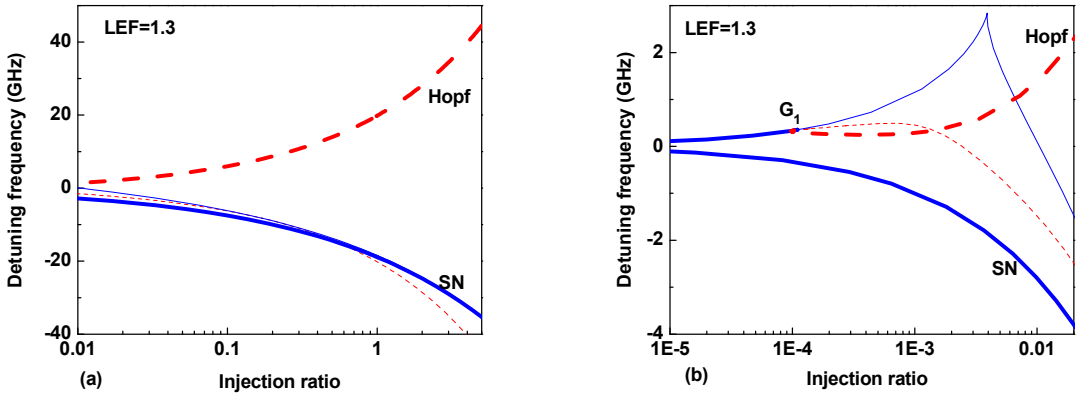

Figure 3. Injection-locking diagrams as functions of injection ratio R_{inj} and detuning frequency Δf_{inj} with LEF=1.3. The saddle-node (SN, solid) and Hopf bifurcations (dash) are calculated with the continuation software Matcont. The stable locking regime is bounded by the supercritical bifurcations (thick line). The thin lines indicate subcritical bifurcations. Injection ratio in (a) is from 0.01 to 5.0; and in (b) is from 10^{-5} to 0.02.

In order to obtain the stable injection-locking regime we investigated the local bifurcations of the QD laser, namely saddle-node and Hopf bifurcations [22], [23]. The bifurcations can be obtained by an eigenvalue analysis of the fixed point, that is, if a single, real eigenvalue passes through the imaginary axis in the complex plane, one typically finds a saddle-node bifurcation while a pair of complex conjugate eigenvalues passing through the imaginary axis corresponds to a Hopf bifurcation. The bifurcations can be calculated by the so-called numerical continuation which is a powerful method for bifurcation analysis, and it is implemented by the continuation package Matcont in our work. The saddle-node (SN, solid line) and Hopf (dashed line) bifurcations are illustrated in figure 3 with LEF of 1.3. The stable locking regime is bounded by the supercritical bifurcations (thick lines) [24]. The regime is enlarged under high injection level. In figure 3(b), it is noted that intersections of the Hopf and SN curves produce a codimension-two point G_1 where the bifurcations changes from supercritical (subcritical) to subcritical (supercritical) along both the Hopf and SN curves. It is worth noting that the laser is known to generate complicated dynamics around this codimension-two point in its vicinity [24]. Besides, it is stressed that the subcritical bifurcation cannot be detected in experiments; nevertheless, it is needed for understanding the global dynamical bifurcations [25].

Figure 4 shows the modulation response under various detuning conditions. It is well known that the injection-locked lasers are identified by three regimes: under negative detuning (-5 GHz), the laser exhibits a linear response since it is over-damped, while hile under zero detuning, the laser is characterized by a broadband and flat response, whose 3-dB bandwidth (12.3 GHz) is about 5.9 fold improved compared to that of the free-running case (2.1 GHz). For the positive frequency detuning (5 GHz), the modulation response exhibits a higher resonance frequency associated with a sharp peak and a large pre-resonance frequency dip. It is proposed that the mechanism for the enhanced resonance frequency in the injection locked semiconductor lasers originates from the interference between the locked field and the shifted cavity-resonance field, while the relaxation oscillation results from the interaction between carriers and photons in the free-running case [26]-[28].

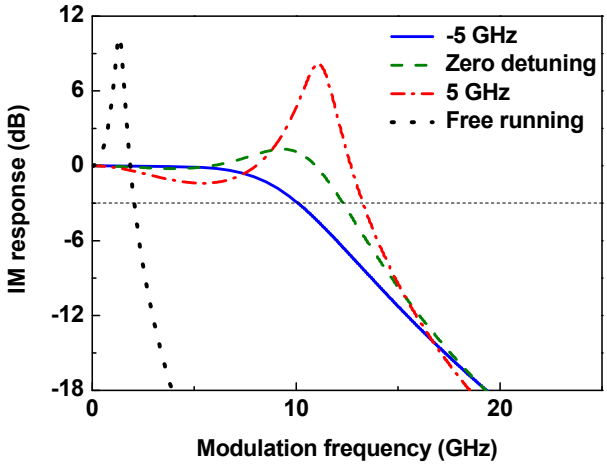

Figure 4. Modulation response under various frequency detuning conditions at -5 GHz (solid line), 0 GHz (dashed line) and 5 GHz (dash-dot line).

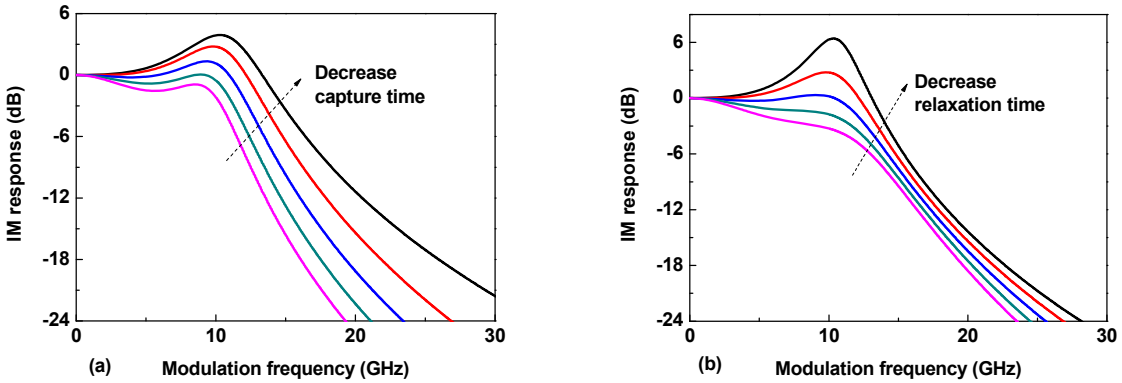

Figure 5. Modulation response under zero detuning. (a) various capture times (2.5 ps, 7.5 ps, 12.6 ps, 17.6 ps and 22.6 ps) at a fixed relaxation time of 3.5 ps; (b) various relaxation times (1.2 ps, 3.5ps, 5.8 ps, 8.1 ps and 10.4 ps) at a fixed capture time of 7.5 ps.

Figure 5 presents the modulation response under zero detuning with various carrier capture times (a) as well as various carrier relaxation times (b). Both large capture and relaxation rates enhance the modulation bandwidth. The calculated bandwidth increases from 10.4 GHz with a capture time of 22.6 ps to 14.8 GHz with a capture time of 2.5 ps. In contrast, for relaxation times of 10.4 ps and 1.2 ps, the calculated 3-dB bandwidths are 9.2 GHz and 14.2 GHz, respectively. Besides, calculations show that the resonance peak is increased as well. Similar effect occurs for the negative detuning (-5 GHz) case as is shown in figure 6.

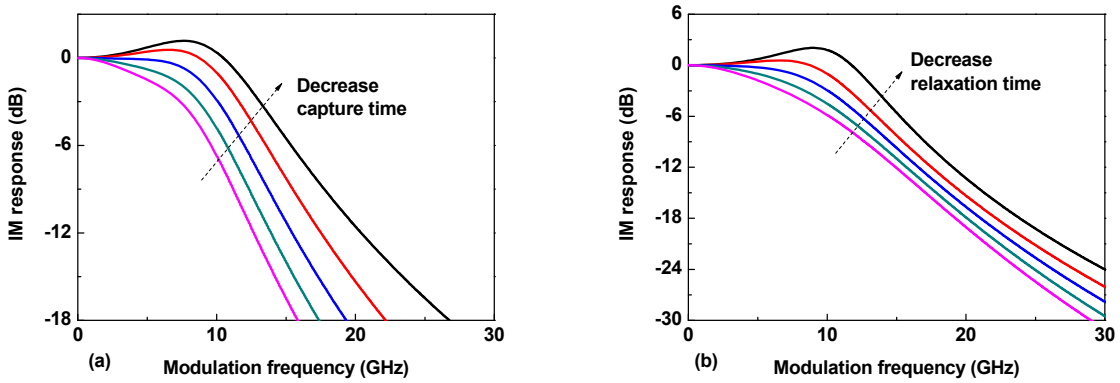

Figure 6. Modulation response under negative detuning at -5 GHz. (a) various capture times (2.5 ps, 7.5 ps, 12.6 ps, 17.6 ps and 22.6 ps) at a fixed relaxation time of 3.5 ps; (b) various relxation times (1.2 ps, 3.5ps, 5.8 ps, 8.1 ps and 10.4 ps) at a fixed capture time of 7.5 ps.

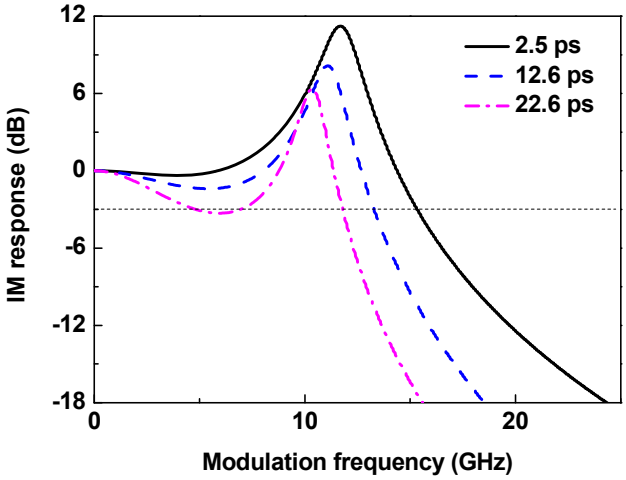

Figure 7. Impacts of carrier capture time at a fixed relaxation time of 3.5 ps under positive detuning (5 GHz).

Table 2. poles and zeros (GHz) for various capture times in figure 7

t (ps)	p_1	p_2	p_3	p_4	p_5	z_1	f_{3dB}
2.5	-5.82±j73.70		-34.48	-292.00	-335.94	-72.75	15.4
12.6	-5.13±j70.04		-31.44	-61.54	-331.30	-71.38	13.3
22.6	-4.01±j65.21		-26.83	-36.87	-330.03	-68.40	11.8

For the positive detuning case, figure 7 shows the IM response with various carrier capture times assuming a fixed relaxation time of 3.5 ps. The modulation bandwidth is enhanced with a faster carrier capture rate. Besides, simulations also point out that a shorter capture time is beneficial to reduce the frequency dip amplitude, which can even be eliminated like the 2.5 ps case. According to the Bode plot, this effect is attributed to the increased pole value $|p_4|$, which becomes larger than the zero value $|z_1|$ (see table 2). However, this frequency dip reduction is accompanied with an increase of the peak amplitude, which can be controlled by the injection strength as shown in figure 6. So increasing the carrier capture rate combined with a high injection ratio can be beneficial to the enhancement of the modulation response. The damping factor Γ and the resonance frequency f_R can be extracted from the complex poles $p_{1,2}$ according to the definition $p_{1,2} = -\Gamma/2 \pm j2\pi f_R$ [2]. In table 2, it is proved that both the resonance frequency and the damping factor increase with the decreased capture time. Figure 8 illustrates the IM response with various carrier relaxation times assuming a fixed capture time of 7.5 ps. In contrast to the case with various capture times, the 3-dB bandwidth is found

nearly unchanged. However, due to the smaller value of $|z_1|-|p_3|$ (see table 3), an almost complete suppression of the pre-resonance dip is also predicted, meanwhile a larger resonance peak amplitude is observed. Inversely to the trend with various capture times, both the resonance frequency and the damping factor are reduced with decreased relaxation time.

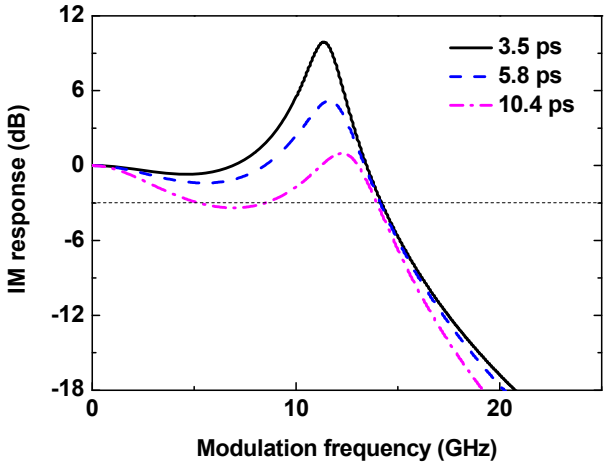

Figure 8. Impacts of carrier relaxation time at a fixed capture time of 7.5 ps under positive detuning (5 GHz).

Table 3. poles and zeros (GHz) for various relaxation times in figure 8

t (ps)	p_1 p_2	p_3	p_4	p_5	z_1	f_{3dB}
3.5	-5.44±j71.75	-32.99	-100.15	-332.07	-71.88	14.2
5.8	-8.43±j74.20	-29.81	-99.58	-200.43	-71.76	14.2
10.4	-10.21±j79.00	-24.03	-97.18	-116.68	-71.21	14.0

4. CONCLUSION

Based on a semi-analytical approach, the modulation response of an optical injection-locked QD laser is modelled taking into account the carrier dynamics in the WL, ES and GS. The influences of carrier capture and relaxation rates on the modulation response are investigated. Large capture and relaxation rates are favourable to enhance both the modulation bandwidth and the resonance peak. Furthermore, it is helpful to suppress or even eliminate the pre-resonance dip in the modulation response under positive detuning, which is desirable for further enhancing the modulation bandwidth. Besides, large capture time reduces both the resonance frequency and the damping factor while relaxation time contributes inversely. Since both the carrier rates can be manipulated via band engineering, these results can be leveraged to our benefits to engineer QD lasers with enhanced dynamical properties under optical injection for radio-over-fibre and cable-access TV applications.

ACKNOWLEDGMENTS

Dr. Frédéric Grillot's research is supported in part by the European Office of Aerospace Research and Development (EOARD) under grant FA8655-12-1-2093. Cheng Wang's work is supported by China Scholarship Council.

REFERENCES

[1] Naderi, N. A., Pochet, M., Grillot, F., Terry, N. B., Kovanis, V., and Lester, L. F., "Modeling the injection-locked behavior of a quantum dash semiconductor laser," IEEE J. Sel. Top. Quantum Electron. 15(3), 563-571 (2009).
[2] Lau, E. K., Sung, H. K., and Wu, M. C., "Frequency response enhancement of optical injection-locked lasers," IEEE J. Quantum Electron. 40(1), 90-99 (2008).
[3] Simpon, B. T., and Liu, M. J., "Bandwidth enhancement and broadband noise reduction in injection-locked semiconductor lasers," IEEE photon. Technol. Lett. 7(7), 709-711 (1995).
[4] Yabre, G., "Effect of relatively strong light injection on the chirp-to-power ration and the 3 dB bandwidth of directly modulated semiconductor lasers," J. Lightwave Tech. 14(10), 2367-2373 (1996).

[5] Liu, M. J. *et al*, "Modulation bandwidth, noise and stability of a semiconductor laser subject to strong injection locking," IEEE photon. Technol. Lett. 9(10), 1325-1327 (1997).
[6] Chen, F. H., Liu, M. J., and Simpson, B. T., "Response characteristics of direct current modulation on a bandwidth enhanced semiconductor laser under strong injection locking," Opt. Commun. 173, 349-355 (2000).
[7] Liu, G. T., Stintz, A., Li, H., Malloy, K. J., and Lester, L. F., "Extremely low room-temperature threshold current density diode lasers using InAs dots in InGaAs quantum well," Electron. Lett. 35(14), 1163-1164 (1999).
[8] Mikhrin, S. S. *et al*,"High power temperature-insensitive 1.3 μm InAs/InGaAs/GaAs quantum dot lasers," Semicond. Sci. Technol. 20(5), 340-345 (2005).
[9] Saito, H., Nishi, K., Kamei, A., and Sigou, S., "Low chirp observed in directly modulated quantum dot lasers," IEEE Photonics Technol. Lett. 12(10), 1298-1230 (2000).
[10] Schneider, H. C., Chow, W. W, and Koch, S., W., "Anomalous carrier-induced dispersion in quantum-dot active media," Phys. Rev. B 66(4), 041310 (2002).
[11] Wang, C., Grillot, F., and Even J., "Impacts of wetting layer and excited state on the modulation response of quantum dot lasers," IEEE J. Quantum Electron. 48(9), 1144-1150 (2012).
[12] Lingnau, B., Ludge, K., Chow, W. W., and Scholl, E., "Influencing modulation properties of quantum-dot semiconductor lasers by carrier lifetime engineering," Appl. Phys. Lett. 101(13), 131107 (2012).
[13] Pausch, J., Otto, C., Tylaite, E., Majer, N., Scholl, E., and Ludge, K., "Optically injected quantum dot lasers: impact of nonlinear carrier lifetimes on frequency-locking dynamics," New Journal of Physics 14, 053018 (2012).
[14] Olejniczak, L., Panajotov, K., Thienpont, H., and Sciamanna, M., "Self-pulsations and excitability in optically injected quantum-dot lasers: Impact of the excited states and the spontaneous emission noise," Physical Review A 82(2), 023807 (2010).
[15] Miska, P., Even, J., Marie, X., and Dehaese, O., "Electronic structure and carrier dynamics in InAs/InP double-cap quantum dots," Appl. Phys. Lett. 94, 061916 (2009).
[16] Miska, P., Even, J., Dehaese, O., and Marie, X., "Carrier relaxation dynamics in InAs/InP quantum dots," Appl. Phys. Lett. 92, 191103 (2008).
[17] Cornet, C., *et al*, "Time-resolved pump-probe in 1.55 μm InAs/InP quantum dots under high resonant excitation," Appl. Phys. Lett. 88, 171502 (2006).
[18] Cornet, C., Levallois, C., Caroff, P., Folliot, H., Labbe, C., Even, J., Corre, L. C., and Loualiche, S., "Impact of the capping layers on the lateral confinement in InAs/InP quantum dots for 1.55 μm laser applications studied by magneto-photoluminescence," Appl. Phys. Lett. 87, 233111 (2005).
[19] Grillot, F., Veselinov, K., Gioannini, M., Montrosset, I., Even, J., Piron, R., Homeyer, E., and Loualiche, S., "Spectral analysis of 1.55-μm InAs-InP(113)B quantum-dot lasers based on a multipopulation rate equations model," IEEE J. Quantum Electron. 45(7), 872-878 (2009).
[20] Coldren, L. A., and Corzine, S. W., [Diode Lasers and Photonic Integrated Circuits], John Wiley & Sons, New York, 195-204 (1995).
[21] Martinez, A. *et al*, "Dynamic properties of InAs/InP(311B) quantum dot Fabry-Perot lasers emitting at 1.52-μm," Appl. Phys. Lett. 93, 021101 (2008).
[22] Wieczorek, S., Simpson T. B., Krauskopf, B., and Lenstra, D., "Global quantitative predications of complex laser dynamics," Physical Review E 65, 045207 (2002).
[23] Wieczorek, S., Krauskopf, B., Simpson, T. B., and Lensra, D., "The dynamical complexity of optically injected semiconductor lasers," Physics Reports 416, 1-128 (2005).
[24] Wieczorek, S., Krauskopf, B., and Lenstra, D., "A unifying view of bifurcations in a semiconductor laser subject to optical injection," Optics Communications 172, 279-295 (1999).
[25] Wieczorek, S., Simpson, T. B., Krauskopf, B., and Lenstra, D., "Bifurcation transitions in an optically injected diode laser: theory and experiment," Optics Communications 215, 125-134 (2003).
[26] Simpson, T. B., and Liu, J. M., "Small-signal analysis of modulation characteristics in a semiconductor laser subject to strong optical injection," IEEE J. Quantum Electron. 32, 1456-1468 (1996).
[27] Simpson, T. B., and liu, J. M., "Enhanced modulation bandwidth in injection-locked semiconductor lasers," IEEE photon. Technol. Lett. 9, 1322-1324 (1997).
[28] Murakami, A., Kawashima, k., and Atsuki, K., "Cavity resonance shift and bandwidth enhancement in semiconductor lasers with strong light injection," IEEE J. Quantum Electron. 39(10), 1196-1204 (2003).